

Engineering decoherence in Josephson persistent-current qubits

Measurement apparatus and other electromagnetic environments

Caspar H. van der Wal ^a, F. K. Wilhelm ^b, C. J. P. M. Harmans, and J. E. Mooij

Department of Applied Physics and Delft Institute for Micro Electronics and Submicron Technology (DIMES),
Delft University of Technology, P. O. Box 5046, 2600 GA Delft, the Netherlands

the date of receipt and acceptance should be inserted later

Abstract. We discuss the relaxation and dephasing rates that result from the control and the measurement setup itself in experiments on Josephson persistent-current qubits. For control and measurement of the qubit state, the qubit is inductively coupled to electromagnetic circuitry. We show how this system can be mapped on the spin-boson model, and how the spectral density of the bosonic bath can be derived from the electromagnetic impedance that is coupled to the qubit. Part of the electromagnetic environment is a measurement apparatus (DC-SQUID), that is permanently coupled to the single quantum system that is studied. Since there is an obvious conflict between long coherence times and an efficient measurement scheme, the measurement process is analyzed in detail for different measurement schemes. We show, that the coupling of the measurement apparatus to the qubit can be controlled *in situ*. Parameters that can be realized in experiments today are used for a quantitative evaluation, and it is shown that the relaxation and dephasing rates that are induced by the measurement setup can be made low enough for a time-resolved study of the quantum dynamics of Josephson persistent-current qubits. Our results can be generalized as engineering rules for the read-out of related qubit systems.

PACS. PACS-03.67.Lx Quantum computation – PACS-05.40.-a Fluctuation phenomena, random processes, noise, and Brownian motion – PACS-74.50.+r Proximity effects, weak links, tunneling phenomena, and Josephson effects – PACS-85.25.Dq Superconducting quantum interference devices (SQUIDS)

1 Introduction

The dynamics of electromagnetic circuits and other macroscopic objects is usually well described by classical laws; quantum coherent phenomena like superposition states are usually not observed in macroscopic systems. The founders of the quantum mechanical theory already recognized that there is in fact a conflict between a straight forward extrapolation of quantum mechanics to a macroscopic scale, and the laws of classical physics that govern the macroscopic world. In particular, this concerns the possibility of quantum superpositions of collective coordinates (i. e. center-of-mass-like coordinates) of objects that are much bigger than the atomic scale. These difficulties were first presented by Schrödinger [1], and are now known as Schrödinger's cat paradox. Schrödinger's discussion of the cat in the box was clearly meant as a *gedanken* experiment. Only several decades later, after the discovery of the Josephson effect,

it was recognized that the validity of quantum mechanics for a macroscopic degree of freedom could be tested in *real* experiments [2].

In 1980, Leggett pointed out that cryogenic and microfabrication technologies had advanced to a level where macroscopic Schrödinger's cat states could possibly be realized in small superconducting loops that contain Josephson tunnel junctions [3,4]. In such systems, the Josephson phase (or equivalently, the persistent supercurrent in the loop) is a collective coordinate for the Cooper-pair condensate, and it is conjugate to a variable which describes the charge difference across the Josephson tunnel junction. However, while the analysis of the isolated quantum system shows that superpositions of the macroscopic coordinates might very well occur in these loops, it is by no means obvious that such behavior can also be demonstrated experimentally. Such superposition states are extremely fragile, reflecting the tendency of macroscopic systems towards classical behavior. Besides decoherence from a weak coupling to the environmental degrees of freedom inside the solid-state device (which is believed to be very much suppressed at low temperatures due to the energy gap for quasiparticle excitations in superconductors), also the fact that the loop is not isolated

^a Present address: Department of Physics, Harvard University, 17 Oxford Street, Cambridge, MA 02138, USA. E-mail: cvanderwal@cfa.harvard.edu

^b Present address: Sektion Physik and CeNS, Ludwig-Maximilians Universität, Theresienstr. 37, 80333 Munich, Germany

but permanently placed in an experimental setup may hinder attempts to study macroscopic quantum coherence. Nevertheless, interesting results with evidence for macroscopic quantum tunneling, energy level quantization and coherent dynamics between quantum levels were obtained with systems where the Josephson phase coordinate is trapped in a metastable well (for an overview see [5,6,7,8,9,10]). Also with systems where the energy scale for single-charge effects is higher than, or comparable to the energy scale for the Josephson effect, quantum coherent dynamics has recently been demonstrated [11,12]. In Josephson junction loops, quantum superposition states of persistent currents have been demonstrated spectroscopically [13,14]. However, time-resolved experiments that prove quantum-coherent oscillations between macroscopically-distinct persistent-currents states in the sense of Ref. [4] have not been reported yet.

Whether such experiments can be realized at all has been intensively discussed in the literature [15], without consensus being reached. However, a detailed analysis with estimates based on measurement techniques that can be realized in experiments *today*, has been discussed very little. The quantum coherent dynamics observed with the other Josephson junction systems (such as Cooper pair boxes [11,12] or single junctions [9,10]), indicates that it might be possible to obtain similar experimental results with Josephson persistent-current loops. Efforts in this direction were stimulated by the prospect that it might be possible to realize a quantum computer with superconducting Josephson devices [16,17,18,19,20,21]. An important advantage of a Josephson quantum computer would be that, if accurate quantum coherent control of elementary units would be possible, it would be a system that can be extended to one containing a very large number of quantum bits (qubits). The large size of the qubits allows for individual (local) control and readout of the qubits and qubit-qubit couplings.

In this article we analyze the feasibility of demonstrating quantum coherent dynamics of Josephson persistent currents with experimental techniques for manipulating and reading qubit states that can be realized in the laboratories *today* (i. e. assuming the available techniques for device fabrication, cryogenics, microwave applications and electronic filtering). Such mesoscopic solid-state experiments suffer from the fundamental difficulty that one cannot avoid that an electronic measuring device is permanently coupled to the *single* quantum system that is studied [22]. We will not consider future measurement techniques which may couple less directly to the qubit. A meter must be present in any useful experiment, and, unlike experiments with for instance photons, this means that a measuring device must be permanently located very close to the solid-state quantum bit (e. g. fabricated on the same chip). With such a setup, there is obviously a conflict between an efficient measurement scheme with a strong measurement, and long decoherence times in the quantum system that is studied. For successful experiments in this direction, a detailed understanding of the measurement scheme is therefore needed such that the decoher-

ence that is induced by the setup itself can be reduced to an acceptable level.

Obviously, there exist many other sources of decoherence for Josephson qubits that one should worry about as well. The critical current of the junctions may show telegraph noise [23], which would give rise to decoherence similar to what is described in Ref. [24]. Moreover, it has been stressed that a very high number of spin degrees of freedom is usually present in the solid state environment that may decohere Josephson qubits (see the work by Prokof'ev and Stamp [25,26] on the spin-bath, and Ref. [27] for estimates for persistent-current qubits). Another example is decoherence from quasiparticles that effectively shunt the junction [28]. These effects themselves are very interesting for further study. However, a study of for example the dephasing due to spin impurities remains impossible as long a reliable and well-understood measurement scheme for the loop's quantum dynamics is not available. Therefore, we will concentrate here on dephasing and mixing due to the experimental wiring and the measurement scheme itself.

Our analysis mainly focuses on experiments with the three-junction persistent-current qubit proposed by Mooij *et al.*, [19,20,14], in a setup where they are measured by underdamped DC-SQUID magnetometers (in this article we will reserve the word SQUID for the measuring DC-SQUID (Fig. 1a), and not use it for the three-junction qubit (Fig. 1, center)). The decohering influence of the inductively coupled DC-SQUID is analyzed as well as decoherence that results from inductive coupling to on-chip control lines for applying microwave signals and local magnetic fields. Model descriptions of the experimental setup will be mapped on the spin-boson model, such that we can use expressions for the relaxation and dephasing rates from the spin-boson literature. The typical experimental situations will be described quite extensively to justify the models and the approximations used. The results will be worked out quantitatively, and we will evaluate whether we can realize mixing and dephasing rates that are compatible with measurement schemes based on DC-SQUIDS. The design criteria developed in this work are more general and should also be of interest for experiments on loops with a single Josephson junction [13], and quantum circuits where the charge degree of freedom is measured, as Josephson charge quantum bits [18,21] and quantum dots [29]. In a more general context the value of this work is that it presents in detail an example of a measurement process on a single quantum system in which the decoherence enhances with increasing measurement strength. The issues discussed here are an example of experimental difficulties that will unavoidably play a role in many realizations of quantum computers.

1.1 Outline

In section 2 we will summarize a theoretical description of the Josephson persistent-current qubit, and the spin-boson theory that will be applied in our analysis. Section 3 presents a description of the measurement process with

the DC-SQUIDS, and a typical scheme for coupling the qubit to the on-chip control lines. In section 4 we work out the qubit's relaxation and dephasing rate that result from the coupling to a switching DC-SQUID. This is worked out quite extensively and the definitions presented in this section are also used in section 5. Two measurement scenarios with different types of electromagnetic shunt circuits for the DC-SQUID will be compared. A short analysis of the decoherence due to the coupling to on-chip control lines is presented in section 5. Section 6 presents a few control techniques that can improve decoherence rates.

2 Qubit Hamiltonian and theory for relaxation and dephasing

This work aims at calculating relaxation (mixing) rates and dephasing (decoherence) rates for a Josephson persistent-current qubit which result from its inductive coupling to the measurement setup. The measurement setup is formed by a DC-SQUID and control lines, which are attached to leads and coupled to filters and electronics (Fig. 1). This setup will be modeled as a macroscopic quantum two-level system (central spin) that is coupled to a linear electromagnetic impedance $Z_t(\omega)$, where ω the angular frequency. The impedance $Z_t(\omega)$ forms an oscillator bath and can be described by a set of LC oscillators. This allows for mapping the problem on the spin-boson model: a central spin- $\frac{1}{2}$ system that is coupled to a bosonic bath [30,31]. The parameters of the bath will be derived from the Johnson-Nyquist noise from $Z_t(\omega)$. In this section we will first introduce the qubit Hamiltonian and physical properties of the qubit, and then summarize the spin-boson expressions for relaxation and dephasing.

2.1 Qubit properties and Hamiltonian

The three-Josephson junction qubit [19,20,14] is a low-inductance superconducting loop which contains three Josephson tunnel junctions (Fig. 1). By applying an external flux Φ_q a persistent supercurrent can be induced in the loop. For values where Φ_q is close to a half-integer number of superconducting flux quanta Φ_0 , two states with persistent currents of opposite sign are nearly degenerate but separated by an energy barrier. We will assume here that the system is operated near $\Phi_q = \frac{1}{2}\Phi_0$. Classically, the persistent currents have here a magnitude I_p . Tunneling through the barrier causes a weak coupling between the two states, and at low energies the loop can be described by a Hamiltonian in the form of a two-level system [19,20,14],

$$\hat{H}_q = \frac{\varepsilon}{2}\hat{\sigma}_z + \frac{\Delta}{2}\hat{\sigma}_x, \quad (1)$$

where $\hat{\sigma}_z$ and $\hat{\sigma}_x$ are Pauli spin operators. The two eigen vectors of $\hat{\sigma}_z$ correspond to states that have a left or a right circulating current and will be denoted as $|L\rangle$ and $|R\rangle$. The energy bias $\varepsilon = 2I_p(\Phi_q - \frac{1}{2}\Phi_0)$ is controlled by the externally applied field Φ_q . We follow [32] and define

Δ as the tunnel splitting at $\Phi_q = \frac{1}{2}\Phi_0$, such that $\Delta = 2W$ with W the tunnel coupling between the persistent-current states. This system has two energy eigen values $\pm\frac{1}{2}\sqrt{\Delta^2 + \varepsilon^2}$, such that the level separation ν gives

$$\nu = \sqrt{\Delta^2 + \varepsilon^2}. \quad (2)$$

In general Δ is a function of ε . However, it varies on the scale of the single junction plasma frequency, which is much above the typical energy range at which the qubit is operated, such that we can assume Δ to be constant for the purpose of this paper.

In the experiments Φ_q can be controlled by applying a magnetic field with a large superconducting coil at a large distance from the qubit, but for local control one can apply currents to superconducting control lines, fabricated on-chip in the direct vicinity of the qubit. The qubit's quantum dynamics will be controlled with resonant microwave pulses (i. e. by Rabi oscillations). The proposed operation point is at $\varepsilon \approx 5\Delta$, which was analyzed to be a good trade-off between a system with significant tunneling, and a system with σ_z -like eigen states that can be used for qubit-qubit couplings and measuring qubit states [19,20]. For optimal microwave control the qubit will be placed in a small off-resonant cavity, and the microwave signals will be applied through on-chip superconducting control lines (i. e. the magnetic component of the fields from microwave currents will be used). The qubit has a magnetic dipole moment as a result of the clockwise or counter-clockwise persistent current. The corresponding flux in the loop is much smaller than the applied flux Φ_q , but large enough to be detected with a SQUID. This will be used for measuring the qubit states. For our two-level system Eq. 1, this means that both manipulation and readout couple to $\hat{\sigma}_z$. Consequently, the noise produced by the necessary circuitry will couple in as flux noise and hence couple to $\hat{\sigma}_z$, giving ϵ a small, stochastically time-dependent part $\delta\epsilon(t)$. Our system also has electric dipole moments, represented by $\hat{\sigma}_x$. These couple much less to the circuitry and will hence not be discussed here.

2.2 Spin-boson theory for relaxation and dephasing

For defining the relaxation and dephasing rates, the state of the qubit is described with a reduced density matrix $\bar{\rho}$, in the basis which is spanned by the eigen vectors of $\hat{\sigma}_z$ in (1), i.e. by the semiclassical states with well-defined left (L) or right (R) circulating current

$$\bar{\rho} = \begin{pmatrix} \rho_{L,L} & \rho_{R,L} \\ \rho_{L,R} & \rho_{R,R} \end{pmatrix}. \quad (3)$$

We will concentrate our discussion on the undriven case. The qubit dynamics consists of quantum-coherent oscillations, which decay on a time-scale $\tau_\phi = \Gamma_\phi^{-1}$, the dephasing time. This dephasing is superimposed on an energy relaxation mechanism on a larger timescale $\tau_r = \Gamma_r^{-1}$, the relaxation time. This combined decoherence process brings the system into an incoherent thermal mixture of its

energy eigen states. Expressed in the basis of these eigen states, the off-diagonal terms (coherences) of the density matrix $\bar{\rho}$ go to zero on the time scale of τ_ϕ , whereas the diagonal terms (populations) decay in τ_r to the Boltzmann factors. For estimating Γ_r and Γ_ϕ we will work from the systematic weak-damping approximation (SWDA) developed by Grifoni *et al.* [32], which covers recent theoretical progress for the spin-boson theory. Grifoni *et al.* calculated expressions for Γ_r and Γ_ϕ for a spin-boson system in which the coupling to the environment is dominated by bilinear coupling terms between $\hat{\sigma}_z$ and the bath coordinates. This is a good approximation for a quantum two-level system that is only weakly damped by the environment.

In our case the bath is formed by the impedance $Z_t(\omega)$, and can be described by a set of LC oscillators with flux coordinates $\hat{\Phi}_i$, conjugate charge coordinates \hat{Q}_i , and Hamiltonian

$$\hat{H}_{bath} = \sum_i \left(\hat{\Phi}_i^2 / 2L_i + \hat{Q}_i^2 / 2C_i \right). \quad (4)$$

The flux produced by the qubit will shift the flux $\hat{\Phi}_i$ in each LC oscillator. The coupling Hamiltonian is

$$\hat{H}_{q-bath} = \frac{\hat{\sigma}_z}{2} \sum_i c_i \hat{\Phi}_i, \quad (5)$$

where c_i is the coupling strength to the i -th oscillator. In this model the influence of the oscillator bath on the qubit can be captured in the environmental spectral density function

$$J(\omega) = \frac{\pi}{2\hbar} \sum_i (c_i^2 / C_i \omega_i) \delta(\omega - \omega_i), \quad (6)$$

where ω_i the resonance frequency of the i -th oscillator. The dense spectrum of the degrees of freedom in the electromagnetic environment allows for treating $J(\omega)$ as a continuous function.

From now on, we focus on the low-damping limit, $J(\omega) \ll \omega$. Thus, the energy-eigenstates of the qubit Hamiltonian, Eq. 1, are the appropriate starting point of our discussion. In this case, the relaxation rate Γ_r (and relaxation time τ_r) are determined by the environmental spectral density $J(\omega)$ at the frequency of the level separation ν of the qubit

$$\Gamma_r = \tau_r^{-1} = \frac{1}{2} \left(\frac{\Delta}{\nu} \right)^2 J(\nu/\hbar) \coth \left(\frac{\nu}{2k_B T} \right), \quad (7)$$

where T is the temperature of the bath. The dephasing rate Γ_ϕ (and dephasing time τ_ϕ) is

$$\Gamma_\phi = \tau_\phi^{-1} = \frac{\Gamma_r}{2} + \left(\frac{\varepsilon}{\nu} \right)^2 \alpha 2\pi \frac{k_B T}{\hbar}. \quad (8)$$

These expressions have been derived in the context of NMR [33] using a Markov approximation and recently been confirmed by a full path-integral analysis [32].

The second term only contributes for an environment which is Ohmic at low frequencies (i. e. for $J(\omega) \propto \omega$). Here α is a dimensionless dissipation parameter. It is determined by the slope of $J(\omega)$ at low frequencies

$$\alpha = \lim_{\omega \rightarrow 0} \frac{J(\omega)}{2\pi\omega}, \quad (9)$$

which, if $J(\omega)$ is a sufficiently smooth function of ω can usually be taken as $\alpha = \frac{1}{2\pi} \frac{\partial J(\omega)}{\partial \omega}$ at $\omega \approx 0$. These results can be intuitively interpreted: The system can relax by dissipating all its energy ν into an environmental boson. Due to the weakness of the coupling, there are no multi-boson processes. The relaxation also dephases the state. Moreover, dephasing can occur due to the coupling to low-frequency modes which do not change the energy of the system. These expressions for relaxation and dephasing have also been found by studying the Hamiltonian of our qubit coupled to a damped oscillator, using a Markovian master equation approach by Tian *et al.* [34] (based on work by Garg *et al.* [35]).

The expressions (7) and (8) have prefactors $(\frac{\Delta}{\nu})^2$ and $(\frac{\varepsilon}{\nu})^2$ that depend on the tunnel splitting Δ and the energy bias ε . These factors correspond to the angles between noise and eigen states usually introduced in NMR [33] and account for the effect that the qubit's magnetic dipole radiation is strongest where the flux in the qubit $\Phi_q = \frac{1}{2}\Phi_0$ (i. e. $(\frac{\Delta}{\nu})$ maximal), and that the level separation ν is insensitive to flux noise at this point (i. e. $\frac{\partial \nu}{\partial \varepsilon} = (\frac{\varepsilon}{\nu}) \approx 0$). One should know and control $J(\omega)$ at the frequency ν/\hbar for controlling the relaxation, and at low frequencies for controlling the dephasing. In this article we will calculate the noise properties of a few typical experimental environments, and calculate how the noise couples to the qubit. This can be used to define $J(\omega)$ for our specific environments.

3 Measurement setup

This section describes a typical experimental setup for measurements on Josephson persistent-current qubits. Only the parts that are most strongly coupled to the qubit will be worked out (Fig. 1). The first part describes a DC-SQUID magnetometer that is used by measuring its switching current, the second part addresses the use of on-chip superconducting lines for applying magnetic fields to the qubit.

3.1 Switching DC-SQUID

SQUIDs are the most sensitive magnetometers, and they can be operated at very low power consumption [36]. We will consider here the use of a DC-SQUID with a hysteretic current-voltage characteristic (IV), and unshunted junctions that are extremely underdamped. It is used by ramping a current through it and recording the switching current: the bias current at which it switches from the supercurrent branch to a nonzero voltage in its IV (Fig. 2). The switching current is a measure for the magnetic flux in the loop of the SQUID. An important advantage of this scheme is that the SQUID produces before readout very little noise. As long as the SQUID is on the supercurrent branch, it does not produce any shot noise or

Josephson oscillations. If the external noise and interference can be suppressed by filtering, there is only Johnson-Nyquist noise from the low-temperature leads and filtering that the SQUID is connected to. At low frequencies this residual noise has little power since the device is superconducting. Moreover, we will show in section 4 that at low bias currents the effective coupling between this meter and the quantum system is very weak. In comparison, damped non-hysteretic SQUIDs have the problem that the shunt resistors at the junctions also provide a damping mechanism for the qubit. In a hysteretic SQUID there is more freedom to engineer the effective impedance seen by the qubit, and it also has the advantage that the voltage jump at the switching current is much larger [37]. Recently, a similar scheme with a superconducting single-charge device, that can be operated as a switching electrometer has been reported [38,12]. Voltage biased single-electron transistors for quantum measurements have been analyzed in Refs. [39,40,41,42].

For qualitative insight in the measurement process we will present here a simplified description of the SQUIDs noise and dynamics (valid for a DC-SQUID with symmetric junctions and a loop with negligible self inductance). In section 4 it will be worked out in more detail. The supercurrent through the SQUID with a flux Φ in its loop is

$$I_{sq} = 2I_{co} \cos f \sin \varphi_{ext}, \quad (10)$$

where $f = \pi\Phi/\Phi_0$, I_{co} the critical current of the junctions, and φ_{ext} a Josephson phase coordinate. I_{sq} will be distinguished from the applied bias current I_{bias} , as part of the bias current may go into circuitry shunting the SQUID. Insight in the SQUID's response to a bias current is achieved by recognizing that (10) gives steady state solutions ($\partial U/\partial \varphi_{ext} = 0$) for a particle with coordinate φ_{ext} , trapped on a tilted washboard potential (Fig. 3)

$$U = -\frac{\hbar}{2e} (2I_{co} \cos f \cos \varphi_{ext} + I_{sq} \varphi_{ext}). \quad (11)$$

In this picture, the average slope of the potential is proportional to the bias current, and the supercurrent branch of the SQUID's IV corresponds to the particle being trapped in a well. The Josephson voltage across the SQUID $V = \frac{\hbar}{2e} \frac{d\varphi_{ext}}{dt}$ is nonzero for the particle in a running mode. In absence of noise and fluctuations, the SQUID will switch to the running mode at the critical current I_C

$$I_C = 2I_{co} |\cos f|. \quad (12)$$

A DC-SQUID can thus be regarded as a single Josephson junction with a flux-tunable critical current. In practice, noise and fluctuations of φ_{ext} will cause the SQUID to switch before the bias current reaches I_C . This current level will be denoted as the switching current I_{SW} to distinguish it from I_C . It is a stochastic variable, but averaging over repeated recordings of I_{SW} allows for determining f with great accuracy. This naive description can be used to illustrate three important properties of the measurement process with the SQUID.

In the experiment, the electronics for recording the SQUID's IV obtains information about f when the SQUID switches. However, rewriting (10) as

$$\varphi_{ext} = \sin^{-1} \left(\frac{I_{sq}}{2I_{co} \cos f} \right) \quad (13)$$

shows that the SQUID's coordinate φ_{ext} is already correlated (i. e. entangled) with the flux f at current values below I_{SW} . Small voltage fluctuations that result from small plasma oscillations and translations of φ_{ext} will cause dissipation in the electromagnetic environment of the SQUID, which damps the dynamics of φ_{ext} . This means, that in a quantum mechanical sense, the position of φ_{ext} , and thereby f , is measured by the degrees of freedom that form the electromagnetic impedance that is shunting the SQUID (i. e. the leads and filtering between the SQUID and the readout electronics), and that the measurement may in fact take place before it is recorded by a switching event.

Secondly, (13) shows that the SQUID's coordinate φ_{ext} is independent of the flux in the loop ($\partial \varphi_{ext}/\partial f = 0$) for $I_{sq} = 0$. Therefore, in absence of fluctuations of φ_{ext} and current noise, the meter is at zero current effectively "off". In practice this can not be perfectly realized, but it illustrates that the decoherence from the SQUID may be reduced by a large extent at low bias currents.

Thirdly, for bias currents well below I_C , the coordinate φ_{ext} is trapped in a potential that is for small oscillations close to harmonic. The SQUID can in this case be regarded as an inductance

$$L_J = \frac{\hbar}{2e} \frac{1}{\sqrt{4I_{co}^2 \cos^2 f - I_{sq}^2}} \quad (14)$$

(see also (26) below). The noise from the SQUID can here be described by the Johnson-Nyquist noise from the SQUID's Josephson inductance (14) in parallel with the SQUID's environmental impedance (Fig. 3a, b). For high bias currents very close to I_C , the spectrum will have more power and calculating the noise properties will be more complicated. Here non-harmonic terms in the trapping potential become important, and there maybe additional noise from a diffusive motion of φ_{ext} to neighboring wells (Fig. 3c). For hysteretic SQUIDs this regime with diffusive motion of φ_{ext} and switching currents very close to I_C will only occur in SQUIDs with a very specific electromagnetic shunt [43,37]. In many realizations of hysteretic DC-SQUIDs φ_{ext} will escape to a running mode without retrapping in lower wells (Fig. 3d), and I_{SW} can be much lower than I_C . In this case the approximation using (14) should be valid for description of the noise before a switching event.

The statistics of I_{SW} readouts depend strongly on the damping of the dynamics of φ_{ext} by the impedance that is shunting the SQUID. Experimental control over the damping, requires the fabrication of a shunt circuit in the direct vicinity of the SQUID, such that its impedance is well defined up to the frequency of the SQUID's plasma oscillations (microwave frequencies). The shunt circuit is

therefore preferably realized on-chip (Z_{sh} in Fig. 1a). The escape from the well may be thermally activated, but for underdamped systems with low-capacitance junctions quantum tunneling through the barrier can dominate the escape rate at low temperatures. The influence of the damping circuitry on the I_{SW} statistics [6,43,37] is now well understood. A SQUID with very underdamped dynamics usually has I_{SW} values much below I_C , and histograms of a set of I_{SW} recordings will be very wide. This means that one needs to average over many repeated measurements to achieve the required resolution in readout. Thereby, averaging also needs to take place over many repeated experiments on the qubit, such that only a time-ensemble average can be measured. With a shunt that provides high damping at the plasma frequency very narrow switching current histograms can be realized [43,37,12,44,45], that in principle allow for single-shot readout in qubit experiments. While in such a scheme the SQUID's noise will also be enhanced, it is possible to engineer (for realistic fabrication parameters) a shunt impedance that is at the same time compatible with coherent dynamics of the qubit and single-shot readout [38]. The engineering of single-shot readout will not be addressed in detail in this paper.

The main disadvantage of the switching SQUID is that it is not very efficient. During each cycle through the hysteretic IV it is only measuring for a short time. Moreover, the IV is very nonlinear, such that the repetition frequency must be an order lower than the bandwidth of the filters. The filtering that is required for realizing low effective temperatures and the SQUID's shunt circuit have typically a bandwidth well below 1GHz, and the accurate readout electronics set a similar limit to the bandwidth. In practice this limits the repetition frequency to values in the range of 10 kHz [14,46] to 1 MHz [8,38]. More efficient readout may be realized with AC readout techniques (see e. g. Ref. [47]).

The slow operation of the switching DC-SQUID sets requirements for the mixing rate Γ_r of the qubit. It needs be longer than the time required to perform a switching current measurement, which requires a time in the range 1 μ s to 100 μ s. One could go to shorter times by setting the SQUID ready at a high bias current when an experiments on the qubit is started, but it is also needed to have the mixing time longer than the time it takes to ramp the bias current through the range of the switching current histogram. At the same time we should realize that the quantum system is prepared by waiting for it to relax to the ground state, so relaxation times very much longer than 100 μ s will prohibit a high repetition frequency. A high repetition frequency is needed if the signal can only be build up by averaging over many switching events.

The experiments aim at working with many coherent Rabi oscillations with a period of about 10 ns [19]. We therefore aim at engineering SQUIDs that cause a dephasing time that is much longer than 10 ns. The dephasing and relaxation times turn out to be shortest at high bias currents through the SQUID. Unless mentioned otherwise, we will make in this article worst case estimates for the

dephasing and relaxation times using bias current values near the switching current.

3.2 On-chip control lines

An attractive feature of macroscopic qubits is that one can address individual qubits with control signals from microfabricated lines (see also Fig. 1b,c). For persistent-current qubits, for example, a supercurrent through a line that is mainly coupled to one specific qubit can be used for tuning this qubit's energy bias ε . Also, it is convenient to provide the microwave signals for control of the qubit's quantum dynamics using local superconducting lines. If this is realized in a microwave cavity with its first resonance well above the applied microwave frequency, one can apply microwave bursts with fast switch times without being hindered by high- Q electromagnetic modes in the volume that is formed by the cold metallic shielding that surrounds the sample.

Microwave signals can be applied using external microwave sources at room temperature. Alternatively, on-chip oscillators for example based on Josephson junction circuits [48,49] can be applied. High microwave currents in the control lines are achieved by shorting the microwave coax or wave guide close to the qubit with an inductance that has an impedance much lower than the source's output impedance (Fig. 1b). For external microwave sources, the typical level for the output impedance will be that of the available coax technology, typically 50 Ω . With on chip Josephson oscillators the typical output impedance is one order lower. In both cases, it is in practice very tedious to engineer these impedance levels and our analysis below will show that this forms a constraint for qubit experiments: long decoherence times are in conflict with the wish for local qubit control and low power levels of the applied microwave signals.

If one uses external microwave sources at room temperature it is harder than for the quasi DC signals to filter out the high temperature noise. Low effective temperatures can be achieved by a combination of narrow-band microwave filters and strong attenuators at low temperatures.

4 Relaxation and dephasing from a switching DC-SQUID

4.1 Current-phase relations for the DC-SQUID

The DC-SQUID has two phase degrees of freedom, the gauge-invariant phases γ_r and γ_l of the junctions [36]. They are related to the supercurrents through the left and the right junction,

$$\begin{aligned} I_l &= (I_{co} + \frac{\Delta I_{co}}{2}) \sin \gamma_l, \\ I_r &= (I_{co} - \frac{\Delta I_{co}}{2}) \sin \gamma_r. \end{aligned} \quad (15)$$

Here I_{co} is the average of the critical current of the two junctions. A small asymmetry in the junctions' critical

currents is accounted for by $\Delta I_{co} \ll I_{co}$ (typically a few percent). We will work here with the sum and difference phase coordinates φ_{int} and φ_{ext} , which are related by a linear transformation

$$\begin{aligned} \varphi_{ext} &= \frac{\gamma_l + \gamma_r}{2} \\ \varphi_{int} &= \frac{\gamma_l - \gamma_r}{2} \end{aligned} \Leftrightarrow \begin{aligned} \gamma_l &= \varphi_{ext} + \varphi_{int} \\ \gamma_r &= \varphi_{ext} - \varphi_{int} \end{aligned} \quad (16)$$

The new phase coordinates are related with the current passing through the SQUID I_{sq} and the circulating current in the SQUID I_{cir}

$$\begin{aligned} I_{sq} &= I_l + I_r \\ I_{cir} &= \frac{I_l - I_r}{2} \end{aligned} \Leftrightarrow \begin{aligned} I_l &= \frac{1}{2} I_{sq} + I_{cir} \\ I_r &= \frac{1}{2} I_{sq} - I_{cir} \end{aligned} \quad (17)$$

yielding the following current-phase relation for I_{sq} and I_{cir}

$$I_{sq} = 2I_{co} \cos \varphi_{int} \sin \varphi_{ext} + \Delta I_{co} \sin \varphi_{int} \cos \varphi_{ext} \quad (18)$$

$$I_{cir} = I_{co} \sin \varphi_{int} \cos \varphi_{ext} + \frac{1}{2} \Delta I_{co} \cos \varphi_{int} \sin \varphi_{ext} \quad (19)$$

We will assume that the DC-SQUID has junctions with a critical current and capacitance that are lower than that of the qubit junctions. In this case, the internal phase φ_{int} follows the flux adiabatically up to time scales much faster than $\frac{\hbar}{\nu}$. We will therefore use

$$\varphi_{int} = \pi \frac{\Phi}{\Phi_0} \stackrel{def}{=} f. \quad (20)$$

4.2 Noise on the qubit from the DC-SQUID resulting in $J(\omega)$

The noise that is induced by the measuring SQUID results from Johnson-Nyquist noise of the total impedance $Z_t(\omega)$ between the leads that are attached to the SQUID. The impedance $Z_t(\omega)$ is formed the SQUID's impedance in parallel with the impedance of the wiring and circuitry that the SQUID is connected to (see the circuit models in Fig. 4). At bias currents well below the critical current I_C , the phase dynamics can be linearized and the SQUID can be modeled as an inductor L_J . The coupling of φ_{ext} to the SQUID's inner degree of freedom φ_{int} and thereby to the qubit slightly alter the effective value for L_J , but the correction it is so small that it can be neglected. The Fourier-transformed power spectrum $\langle \delta V(t) \delta V(0) \rangle_\omega$ of the Johnson-Nyquist voltage fluctuations δV across the SQUID is [31,50]

$$\langle \delta V \delta V \rangle_\omega = \hbar \omega \text{Re}\{Z_t(\omega)\} \coth\left(\frac{\hbar \omega}{2k_B T}\right). \quad (21)$$

We will now calculate how this voltage noise leads to fluctuations $\delta \varepsilon$ of the energy bias on the qubit. As a rule, the spectral density $J(\omega)$ in (6) can then be derived by dividing the expression for $\langle \delta \varepsilon \delta \varepsilon \rangle_\omega$ by $\hbar^2 \coth\left(\frac{\hbar \omega}{2k_B T}\right)$.

The current-phase relations for I_{sq} and I_{cir} can be used for expressing the current fluctuations. The first term of (18) gives

$$\begin{aligned} \frac{dI_{sq}}{dt} &= i\omega I_{sq} \approx 2I_{co} \cos f \cos \bar{\varphi}_{ext} \frac{d\varphi_{ext}}{dt} \\ &= 2I_{co} \cos f \cos \bar{\varphi}_{ext} \frac{2e}{\hbar} V, \end{aligned} \quad (22)$$

where we used $\bar{\varphi}_{ext}$ for the time average of φ_{ext} . With a similar expression for the second term of (18) the current fluctuations in I_{sq} are

$$\delta I_{sq} \approx (2I_{co} \cos f \cos \bar{\varphi}_{ext} - \Delta I_{co} \sin f \sin \bar{\varphi}_{ext}) \delta \varphi_{ext}. \quad (23)$$

The SQUID is usually operated in regions where the average external flux in its loop is between an integer and half-integer number of Φ_0 . At these points $|\cos f| \approx |\sin f|$. Therefore, the second term in (23) can be neglected unless $|I_{co} \cos \bar{\varphi}_{ext}| \lesssim |\Delta I_{co} \sin \bar{\varphi}_{ext}|$. That is, it can be neglected unless the bias current is very high, for which $\sin \bar{\varphi}_{ext}$ approaches 1. For most purposes we can thus use

$$\delta I_{sq} \approx 2I_{co} \cos f \cos \bar{\varphi}_{ext} \delta \varphi_{ext}. \quad (24)$$

This is also used to define L_J by expressing

$$V = L_J \frac{dI_{sq}}{dt}, \quad (25)$$

such that with (22), (20) and (18) L_J should be defined as

$$L_J = \frac{\hbar}{2e} \frac{1}{2I_{co} \cos f \cos \bar{\varphi}_{ext}} = \frac{\hbar}{2e} \frac{1}{\sqrt{4I_{co}^2 \cos^2 f - I_{sq}^2}}. \quad (26)$$

For I_{cir} we get a similar expression as (23)

$$\delta I_{cir} \approx (-I_{co} \sin f \sin \bar{\varphi}_{ext} + \frac{1}{2} \Delta I_{co} \cos f \cos \bar{\varphi}_{ext}) \delta \varphi_{ext}. \quad (27)$$

Using again that the SQUID is operated where $|\cos f| \approx |\sin f|$ shows that the second term in (27) can be neglected unless $|I_{co} \sin \bar{\varphi}_{ext}| \lesssim |\Delta I_{co} \cos \bar{\varphi}_{ext}|$. For δI_{cir} the second term only plays a role at low bias currents in the SQUID for which $\bar{\varphi}_{ext} \approx 0$, and for most purposes we can use

$$\delta I_{cir} \approx -I_{co} \sin f \sin \bar{\varphi}_{ext} \delta \varphi_{ext}. \quad (28)$$

In the above we used $\bar{\varphi}_{ext}$ for the time average of φ_{ext} , but at places where it is not confusing it will be simply denoted as φ_{ext} .

Both noise in I_{sq} and I_{cir} can couple to the qubit, but we will assume that the qubit is mainly sensitive to noise in I_{cir} (as in the experiments in [14], where the qubit was placed symmetrically inside the SQUID's loop) and neglect an inductive coupling to noise in I_{sq} . For a more general approach, coupling to noise in I_{sq} can be treated on a similar footing as noise in I_{cir} , but for all useful sample geometries it should give a contribution to relaxation and dephasing rates that is at most on the same order as that of I_{cir} .

With $i\omega \delta I_{cir} = -\frac{2e}{\hbar} I_{co} \sin f \sin \varphi_{ext} \delta V$ follows for the fluctuations δI_{cir}

$$\langle \delta I_{cir} \delta I_{cir} \rangle_\omega = \left(\frac{2e}{\hbar}\right)^2 \frac{1}{\omega^2} I_{co}^2 \sin^2 f \sin^2 \varphi_{ext} \langle \delta V \delta V \rangle_\omega. \quad (29)$$

The fluctuations in the imposed qubit flux are $\delta \Phi_q = M \delta I_{cir}$, where M the mutual inductance between the SQUID

loop and the qubit loop. This then yields the fluctuations in the energy bias with $\delta\varepsilon = 2I_p\delta\Phi_q$,

$$\langle\delta\varepsilon\delta\varepsilon\rangle_\omega = \left(\frac{2e}{\hbar}\right)^2 \frac{4}{\omega^2} M^2 I_p^2 I_{co}^2 \sin^2 f \sin^2 \varphi_{ext} \langle\delta V\delta V\rangle_\omega \quad (30)$$

where I_p is the amplitude of the circulating current in the qubit in the semiclassical states. Using (18) and (21) and filling in $\frac{\hbar}{2e} = \Phi_0$ this can be written as

$$\langle\delta\varepsilon\delta\varepsilon\rangle_\omega = \hbar (2\pi)^2 \frac{1}{\omega} \left(\frac{MI_p}{\Phi_0}\right)^2 I_{sq}^2 \tan^2 f \times \text{Re}\{Z_t(\omega)\} \coth\left(\frac{\hbar\omega}{2k_B T}\right) \quad (31)$$

The fluctuations $\langle\delta\varepsilon\delta\varepsilon\rangle_\omega$ are the result of the coupling to the oscillator bath, as in (6). This can be used to define $J(\omega)$ for our specific environment,

$$J(\omega) = \frac{(2\pi)^2}{\hbar} \frac{1}{\omega} \left(\frac{MI_p}{\Phi_0}\right)^2 I_{sq}^2 \tan^2 f \text{Re}\{Z_t(\omega)\}. \quad (32)$$

These results show, that although the SQUID is permanently close to the qubit, it may be effectively decoupled if there is no net bias current I_{sq} flowing through the device. The physical reason for this becomes apparent in Eqs. (18) and (19): The SQUID remains mirror symmetric in that case and consequently the fluctuations of the bias current are diverted symmetrically around the arms of the SQUID and do not produce flux noise [51].

4.3 Relaxation times

With (7) and (32) follows the SQUID's contribution to the relaxation rate. It is here expressed as a function of the resonance frequency $\omega_{res} = \nu/\hbar$ at which the qubit is operated,

$$\Gamma_r = \left(\frac{\Delta/\hbar}{\omega_{res}}\right)^2 \frac{(2\pi)^2}{2\hbar} \frac{1}{\omega_{res}} \left(\frac{MI_p}{\Phi_0}\right)^2 I_{sq}^2 \tan^2 f \times \text{Re}\{Z_t(\omega_{res})\} \coth\left(\frac{\hbar\omega_{res}}{2k_B T}\right). \quad (33)$$

In this formula one can recognize a dimensionless factor $\left(\frac{MI_p}{\Phi_0}\right)^2$ which is a scale for how strongly the qubit is coupled to the measuring SQUID. A dissipation factor in the form $I^2 R$ can be recognized in $I_{sq}^2 \tan^2 f \text{Re}\{Z_t(\omega)\}$. The dissipation scales with the absolute value of the current fluctuations, so with I_{sq} , and the expression is independent of the critical current of the SQUID junctions I_{co} (unless $\text{Re}\{Z_t(\omega)\}$ depends on I_{co}). A weak measurement scheme in which the inductive coupling to a DC-SQUID $(MI_p/\Phi_0)^2 \ll 1$ can yield relaxation rates that are very low when compared to a scheme in which leads are directly attached to the loop [52]. A measurement of such a scheme's switching current could also be used for probing the qubit, but the influence of the voltage noise would be dramatically worse.

With the result (33) the relaxation rate for typical sample parameters will be calculated. Sample parameters

similar to our recent experiment [14] are $\omega_{res} = 10$ GHz, $\Delta = 2$ GHz, $\frac{MI_p}{\Phi_0} = 0.002$. It is assumed that a SQUID with $2I_{co} = 200$ nA is operated at $f = 0.75 \pi$ and biased near the switching current, at $I_{sq} = 120$ nA. For $T = 30$ mK the relaxation rate per Ohm environmental impedance is then

$$\tau_r = \Gamma_r^{-1} \approx \frac{150 \mu\text{s} \Omega}{\text{Re}\{Z_t(\omega_{res})\}}. \quad (34)$$

4.4 Engineering $\text{Re}\{Z_t(\omega)\}$ for slow relaxation

In practice the SQUID's resolution is improved by building an on-chip electromagnetic environment. We will consider here a large superconducting capacitive shunt (Fig. 4a, as in our recent experiment [14]). This scheme will be denoted as the *C*-shunted SQUID. As an alternative we will consider a shunt that is a series combination of a large capacitor and a resistor (Fig. 4b). This will be denoted as the *RC*-shunted SQUID. The *C* shunt only makes the effective mass of the SQUID's external phase φ_{ext} very heavy. The *RC* shunt also adds damping at the plasma frequency of the SQUID, which is needed for realizing a high resolution of the SQUID readout (i. e. for narrow switching-current histograms) [37]. The total impedance $Z_t(\omega)$ of the two measurement circuits are modeled as in Fig. 4. We assume a perfect current source I_{bias} that ramps the current through the SQUID. The fact that the current source is non-ideal, and that the wiring to the SQUID chip has an impedance is all modeled by the impedance Z_l . The wiring can be engineered such that for a very wide frequency range the impedance Z_l is on the order of the vacuum impedance, and can be modeled by its real part R_l . It typically has a value of 100Ω . On chip, the impedance is formed by the Josephson inductance L_J in parallel with the shunt circuit (C_{sh} , or the series combination of R_{sh} and C_{sh}). We thus assume that the total impedance $Z_t(\omega)$ can be described as

$$Z_t(\omega) = \left(\frac{1}{i\omega L_J} + \frac{1}{\frac{1}{i\omega C_{sh}} + R_{sh}} + \frac{1}{R_l} \right)^{-1}, \quad (35)$$

where R_{sh} should be taken zero for the *C*-shunt scenario.

The circuits in Fig. 4 are damped *LC* resonators. It is clear from (7) and (32) that one should keep the *LC*-resonance frequency $\omega_{LC} = 1/\sqrt{L_J C_{sh}}$, where $\text{Re}\{Z_t(\omega)\}$ has a maximum, away from the qubit's resonance $\omega_{res} = \nu/\hbar$. For practical values this requires $\omega_{LC} \ll \omega_{res}$ for Aluminum technology (with Niobium-based technology, the regime $\omega_{LC} \gg \omega_{res}$ may be realized [44]). This then gives the circuits a $\text{Re}\{Z_t(\omega)\}$ and $J(\omega)$ as plotted in Fig. 5. For the circuit with the *C* shunt

$$\text{Re}\{Z_t(\omega)\} \approx \begin{cases} \frac{\omega^2 L_J^2}{R_l}, & \text{for } \omega \ll \omega_{LC} \\ R_l, & \text{for } \omega = \omega_{LC} \\ \frac{1}{\omega^2 C_{sh}^2 R_l}, & \text{for } \omega \gg \omega_{LC} \end{cases} \quad (36)$$

For the circuit with the RC shunt

$$\text{Re}\{Z_t(\omega)\} \approx \begin{cases} \frac{\omega^2 L_J^2}{R_l}, & \text{for } \omega \ll \omega_{LC} \\ \lesssim R_l, & \text{for } \omega = \omega_{LC} \ll \frac{1}{R_{sh} C_{sh}} \\ R_l / R_{sh}, & \text{for } \omega = \omega_{LC} \gg \frac{1}{R_{sh} C_{sh}} \\ R_l / R_{sh}, & \text{for } \omega \gg \omega_{LC} \end{cases} \quad (37)$$

The difference mainly concerns frequencies $\omega > \omega_{LC}$, where the C -shunted circuit has a $\text{Re}\{Z_t(\omega)\}$, and thereby a relaxation rate, that is several orders lower than for the RC -shunted circuit.

For a C -shunted circuit with $\omega_{LC} \ll \omega_{res}$ the $\text{Re}\{Z_t(\omega_{res})\} \approx \frac{1}{\omega_{res}^2 C_{sh}^2 R_l}$. This yields for $J(\omega)$ at $\omega > \omega_{LC}$

$$J(\omega) \approx \frac{(2\pi)^2}{\hbar} \frac{1}{\omega^3} \left(\frac{M I_p}{\Phi_0} \right)^2 I_{sq}^2 \tan^2 f \frac{1}{C_{sh}^2 R_l} \quad (38)$$

The factor $1/\omega^3$ indicates a natural cut-off for $J(\omega)$, which prevents the ultraviolet divergence [30,32] and which in much of the theoretical literature is introduced by hand. The RC -shunted circuit has softer cut off $1/\omega$. The mixing rate for the C -shunted circuit is then

$$\Gamma_r \approx \frac{(\Delta/\hbar)^2 (2\pi)^2}{\omega_{res}^5} \frac{(M I_p)^2}{\Phi_0^2} I_{sq}^2 \tan^2 f \times \frac{1}{C_{sh}^2 R_l} \coth \left(\frac{\hbar \omega_{res}}{2 k_B T} \right). \quad (39)$$

Fig. 6 presents mixing times τ_r vs ω_{res} for typical sample parameters (here calculated with the non-approximated version of $\text{Re}\{Z_t(\omega)\}$). With the C -shunted circuit it seems possible to get τ_r values that are very long. They are compatible with the ramp times of the SQUID, but too slow for fast repetition rates. In Fig. 5 one can directly see from the values of $J(\omega)$ that an RC -shunted circuit with otherwise similar parameters yields at $\omega_{res}/2\pi = 10$ GHz relaxation times that are about four orders shorter. For the parameters used here they are in the range of 15 μ s. While this value is close to the desired order of magnitude, one has to be aware of the fact at these high switching current values the linearization Eq. (26) may underestimate the actual noise. In that regime, phase diffusion between different minima of the washboard potential also becomes relevant and changes the noise properties [37,53].

4.5 Dephasing times

At low frequencies $\omega < \omega_{LC}$ the C -shunted and RC -shunted scheme have $\text{Re}\{Z_t(\omega)\} \approx \frac{\omega^2 L_J^2}{R_l}$ such that with (32) and (9)

$$J(\omega) \approx \frac{(2\pi)^2}{\hbar} \omega \left(\frac{M I_p}{\Phi_0} \right)^2 I_{sq}^2 \tan^2 f \frac{L_J^2}{R_l}, \quad (40)$$

$$\alpha \approx \frac{2\pi}{\hbar} \left(\frac{M I_p}{\Phi_0} \right)^2 I_{sq}^2 \tan^2 f \frac{L_J^2}{R_l}. \quad (41)$$

The environment is Ohmic at low frequencies since we have $J(\omega) \propto \omega$. For our sample parameters the second

term in (8) dominates, such that with (41) and for the qubit operated where $\varepsilon \approx \nu$

$$\Gamma_\phi \approx \frac{(2\pi)^2}{\hbar^2} \left(\frac{M I_p}{\Phi_0} \right)^2 I_{sq}^2 \tan^2 f \frac{L_J^2}{R_l} k_B T. \quad (42)$$

Note in (26) that $L_J \propto 1/I_{co}$, such that the dephasing rate (42) does not depend on the absolute value of the current, but on the ratio I_{sq}/I_C . For the typical sample parameters as used in Fig. 5 the dephasing time is about 10 ns, which is too short. However, we can gain a few orders (if Γ_r is low enough) by the fact that we can do the quantum coherent control at low I_{sq} (the previous estimate was calculated for $I_{sq} = 120$ nA, in the switching region). At $I_{sq} = 0$ we find $\Gamma_\phi = 0$ in this linear approximation for the SQUID inductance. At $I_{sq} = 0$ we should therefore estimate the dephasing due to second order terms. However, in practice the dephasing is probably dominated by the second term in (27), which is due to a small asymmetry in the fabricated SQUID junctions of a few percent. This influence can be mapped on a small bias current (a few percent of the critical current, say 5 nA) through the SQUID. Therefore, at $I_{sq} \approx 0$ the dephasing times can be $(\frac{120}{5})^2$ times longer. Furthermore, the factor L_J^2 , as defined in (26), is at 5 nA about a factor 2 lower than at 120 nA. For our parameters this allows for $\tau_\phi \approx 20$ μ s, see also Fig. 7. Further improvement is feasible by making e. g. $R_l = 1$ k Ω , working with a lower mutual inductance M or tuning the qubit close to the degeneracy point, as in [12].

Finally, we would like to mention that in the literature on dissipative two-level systems one often assumes Ohmic dissipation, corresponding to a purely resistive shunt across the junctions of the qubit. For a description of such a system one usually introduces an artificial exponential cut off at frequency ω_c , yielding $J(\omega)$ of the form

$$J(\omega) = \alpha \omega \exp(-\frac{\omega}{\omega_c}). \quad (43)$$

In our case, $J(\omega)$ has substantial internal structure originating from the frequency-dependence of $\text{Re}\{Z_t(\omega)\}$. In order to compare our results to the Ohmic case, we plot in Fig. 5 an Ohmic fit to the actual $J(\omega)$ of the DC SQUID. For the parameters as in Fig. 5 the resemblance is reasonable for a resistive shunt corresponding to $\alpha = 0.00062$, and a cut off $\omega_c = 0.5$ GHz. For low currents, as for the dashed line in Fig. 7 $\alpha = 1 \cdot 10^{-7}$. This corresponds to an extremely underdamped system, with a long dephasing time.

5 Relaxation and dephasing from on-chip control circuits

We will treat here the influence of noise from the microwave leads in a similar way as worked out for the SQUID. Here the total environmental impedance $Z_t(\omega)$ is formed by a 50 Ω coax, that is shorted at the end by a small inductance L_{mw} , see the circuit model in Fig. 8. This inductance L_{mw} has a mutual inductance M_{mw} to the qubit.

The voltage noise is given by (21). The noise leads to fluctuations $\delta\varepsilon$ of the energy bias separation ε as follows. The current noise in L_{mw} is $\delta I_L = \frac{1}{i\omega L_{mw}}\delta V$. The qubit fluctuations in the flux Φ_q are then $\delta\Phi_q = M_{mw}\delta I_L$, and the fluctuations in the energy bias are $\delta\varepsilon = 2I_p\delta\Phi_q$. This gives for the fluctuations $\langle\delta\varepsilon\delta\varepsilon\rangle_\omega$

$$\langle\delta\varepsilon\delta\varepsilon\rangle_\omega = \frac{4\hbar}{\omega} \left(\frac{M_{mw}I_p}{L_{mw}} \right)^2 \text{Re}\{Z_t(\omega)\} \coth\left(\frac{\hbar\omega}{2k_B T}\right) \quad (44)$$

and for the environmental spectral density (6)

$$J(\omega) = \frac{4}{\hbar\omega} \left(\frac{M_{mw}I_p}{L_{mw}} \right)^2 \text{Re}\{Z_t(\omega)\}. \quad (45)$$

The $\text{Re}\{Z_t(\omega)\}$ is that of a first order low-pass LR filter with a -3 dB frequency $\omega_{LR} = R/L$. For the L_{mw} to be effectively a short its impedance ωL_{mw} should be small compared to $50\ \Omega$ at the frequency of the applied microwave radiation (typically 10 GHz), giving $L_{mw} \ll 1\text{ nH}$. This can be realized by making the length of the short line less than about $100\ \mu\text{m}$. This means that all relevant frequencies are below the -3 dB frequency ω_{LR} , and that for both relaxation and dephasing we can approximate

$$\text{Re}\{Z_t(\omega)\} \approx \frac{\omega^2 L_{mw}^2}{R_{mw}} \quad (46)$$

with $R_{mw} = 50\ \Omega$. For $\omega < \omega_{LR}$, $J(\omega)$ is again Ohmic,

$$J(\omega) = \frac{4\omega}{\hbar} \frac{(M_{mw}I_p)^2}{R_{mw}}, \quad (47)$$

and with (9) we find for α

$$\alpha \approx \frac{4}{2\pi\hbar} \frac{(M_{mw}I_p)^2}{R_{mw}}. \quad (48)$$

Note that these results are independent of L_{mw} . A larger L_{mw} leads to enhanced voltage noise, but the resulting current noise is reduced by the same factor. For frequencies below ω_{LR} the current noise is just that of a shorted $50\ \Omega$ resistor. For frequencies higher than ω_{LR} , $\text{Re}\{Z_t(\omega)\} \approx R_{mw}$, such that $J(\omega)$ has a very soft intrinsic $1/\omega$ cut off.

For the relaxation rate (7) as a function of the qubit's resonance frequency ω_{res} we now have

$$\Gamma_r \approx \frac{2\Delta^2}{\hbar^3\omega_{res}} \frac{(M_{mw}I_p)^2}{R_{mw}} \coth\left(\frac{\hbar\omega_{res}}{2k_B T}\right). \quad (49)$$

This has a much weaker dependence on ω_{res} than for the SQUID, results are plotted in Fig. 6. The results are plotted for $M_{mw} = 0.1\text{ pH}$ (further parameters are as used for the SQUID calculations) and for this M_{mw} value the relaxation times are in the required range of about $100\ \mu\text{s}$. The value $M_{mw} \approx 0.1\text{ pH}$ corresponds to a $5\ \mu\text{m}$ loop at about $25\ \mu\text{m}$ distance from the microwave line, and is compatible with the fabrication possibilities and the microwave requirements. With this geometry it is still possible to apply sufficient microwave power for pumping the

qubit's Rabi dynamics at 100 MHz (i. e. pumping with an oscillating Φ_q of about $0.001\ \Phi_0$ [19], which needs an oscillating current of $\frac{0.001\ \Phi_0}{M_{mw}} \approx 20\ \mu\text{A}$, corresponding to 20 nW , i. e. -47 dBm microwave power), while the dissipated microwave power in the attenuators at the refrigerator's base temperature remains well below the typical cooling power of $1\ \mu\text{W}$.

For the second term of the dephasing rate (8) we thus find for the qubit operated where $\varepsilon \approx \nu$

$$\Gamma_\phi \approx \frac{4}{\hbar^2} \frac{(M_{mw}I_p)^2}{R_{mw}} k_B T. \quad (50)$$

Using the same parameters as in the above calculation of the relaxation time we find $\alpha \approx 1 \cdot 10^{-7}$ and for $T = 30\text{ mK}$ the dephasing time is $\tau_\phi \approx 130\ \mu\text{s}$. While this dephasing rate is sufficient for demonstration experiments and promising for applications, we like to note that it is much harder to engineer this dephasing rate as compared to the DC-SQUID dephasing. It is in practice quite tedious to apply microwave technology with impedance levels R_{mw} much higher than $50\ \Omega$, both for externally generated microwaves and on chip generators (it could for instance be increased using a planar impedance transformer [54]). Making M_{mw} smaller requires higher microwave currents, and thereby more microwave dissipation on the mixing chamber. The cooling power per qubit will quite likely remain below $1\ \mu\text{W}$, so much stronger microwave signals from a larger distance is not an option. Moreover, making M_{mw} very small means that the control line is $100\ \mu\text{m}$ or further away from the qubit. In this case, applying microwaves locally to one specific qubit on a chip with several coupled qubits is much harder.

6 Suppressing rates by freezing states and idle states

With additional control techniques the decoherence rates can be made better than the estimates made in the previous sections. These are based on the pre-factors in Eqs. (7) and (8). Bringing the qubit in a so-called idle state ($\varepsilon = 0$) [18] can reduce the dephasing, but not beyond $\Gamma_r/2$ (which is enhanced at $\varepsilon = 0$).

Another useful technique is freezing. Here, the tunnel coupling Δ between the two qubit states is strongly reduced before the measurement process starts with a fast but adiabatic control current [19]. This allows for much slower measurements, thus for weaker coupling to a damped SQUID with very high resolution. Moreover, it has the advantage that the tunnel coupling becomes so weak that the Hamiltonian almost commutes with $\hat{\sigma}_z$. This can improve the correlation between the outcome of $\hat{\sigma}_z$ measurements, and energy states in the case that the calculation states are energy eigen states. However, freezing requires that the qubit junctions are realized as small DC-SQUIDS. This means that $\hat{\sigma}_x$ noise will be strongly enhanced. The influence of this additional noise source can be calculated along the same lines as in [32] and, assuming that it is not correlated with the other noise sources,

add up to the rates we have calculated in this paper. See Fig. 9 for numerical estimates on the possible adiabatic suppression of Δ .

7 Discussion and conclusion

We have developed a scheme for modeling the decoherence of a persistent-current qubit due to its electromagnetic environment. Examples for both control and read-out electronics are worked out quantitatively. We discussed how the dephasing and relaxation rates of the qubit can be derived from the impedance of the electronic circuitry, and provided design criteria for such electronics. In particular, we have shown that even though the readout SQUID is always close to the qubit, it can be effectively decoupled. Our examples show that the present status of experimental technology should allow for the observation of quantum coherent oscillations between macroscopic persistent-current states.

In this final section, we like to point out that the theory that is used is still in development. In particular, an environment with a strongly structured spectrum may violate the weak-coupling Born approximation at its resonance frequencies, but it may also induce weak additional decoherence off-resonance. This situation is hardly accessible with traditional theoretical methods for this problem and alternative approaches such as the flow-equation scheme in [55] may be needed. Furthermore, it is not clear whether the impedance can be described by a single temperature. At low frequencies, noise from parts in the system with a higher temperature can reach the sample. However, the experimental results reported in Ref. [12] indicate, that an analysis of the decoherence of the type we give here gives good predictions of the experimental decoherence time scales in a superconducting qubit.

The authors thank D. Esteve, M. Grifoni, Y. Nakamura, P. C. E. Stamp, A. C. J. ter Haar, L. Levitov, T. P. Orlando, L. Tian, and S. Lloyd for help and stimulating discussions. Financial support by the Dutch Foundation for Fundamental Research on Matter (FOM), the European TMR research network on superconducting nanocircuits (SUPNAN), the USA National Security Agency (NSA) and Advanced Research and Development Activity (ARDA) under Army Research Office (ARO) contract numbers DAAG55-98-1-0369 and P-43385-PH-QC, and the NEDO joint research program (NTDP-98) is acknowledged.

References

1. E. Schrödinger, *Naturwissenschaften* **23**, 807-812, 823-828, 844-849 (1935).
2. P. W. Anderson, in *Lectures on the Many-Body Problem*, E. R. Caianiello, Ed. (Academic Press, New York, 1964), vol. 2, pp. 113-135.
3. A. J. Leggett, *Prog. Theor. Phys. Suppl.* **69**, 80 (1980).
4. A. J. Leggett, A. Garg, *Phys. Rev. Lett.* **54**, 857 (1985).
5. K. K. Likharev, *Sov. Phys. Usp.* **26**, 87 (1983).
6. J. Clarke, A. N. Cleland, M. H. Devoret, D. Esteve, J. M. Martinis, *Science* **239**, 992 (1988).
7. S. Han, R. Rouse, J. E. Lukens, *Phys. Rev. Lett.* **76**, 3404 (1996).
8. P. Silvestrini, V. G. Palmieri, B. Ruggiero, M. Russo, *Phys. Rev. Lett.* **79**, 3046 (1997).
9. Y. Yu, S. Y. Han, X. Chu, S. I. Chu, and Z. Wang, *Science* **296**, 889 (2002).
10. J. M. Martinis, S. Nam, J. Aumentado, and C. Urbina, *Phys. Rev. Lett.* **89**, 117901 (2002).
11. Y. Nakamura, Yu. A. Pashkin, J. S. Tsai, *Nature* **398**, 786 (1999).
12. D. Vion, A. Aassime, A. Cottet, P. Joyez, H. Pothier, C. Urbina, D. Esteve, and M. H. Devoret, *Science* **296**, 886 (2002).
13. J. R. Friedman, V. Patel, W. Chen, S. K. Tolpygo, J. E. Lukens, *Nature* **406**, 43 (2000).
14. C. H. van der Wal *et al.*, *Science* **290**, 773 (2000).
15. C. D. Tesche, *Phys. Rev. Lett.* **64**, 2358 (1990).
16. M. F. Bocko, A. M. Herr, M. J. Feldman, *IEEE Trans. Appl. Supercond.* **7**, 3638 (1997).
17. L. B. Ioffe, V. B. Geshkenbein, M. V. Feigel'man, A. L. Fauchère, G. Blatter, *Nature* **398**, 679 (1999).
18. Yu. Makhlin, G. Schön, A. Shnirman, *Nature* **398**, 305 (1999).
19. J. E. Mooij *et al.*, *Science* **285**, 1036 (1999).
20. T. P. Orlando *et al.*, *Phys. Rev. B* **60**, 15398 (1999).
21. Yu. Makhlin, G. Schön, A. Shnirman, *Rev. Mod. Phys.* **73**, 357 (2001).
22. Alternatively, one could also take an NMR-like approach and measure on an ensemble of loops. This is not discussed in this article.
23. R. T. Wakai and D. J. van Harlingen, *Phys. Rev. Lett.* **58**, 1687 (1987).
24. E. Paladino, L. Faoro, G. Falci, and R. Fazio, *Phys. Rev. Lett.* **88**, 228304 (2002).
25. N. Prokof'ev, P. Stamp, *Rep. Prog. Phys.* **63**, 669 (2000); cond-mat/0001080.
26. N. V. Prokof'ev, P. C. E. Stamp, *Spin-bath mediated decoherence in superconductors*, submitted to *Phys. Rev. Lett.*, (2000); cond-mat/0006054.
27. L. Tian *et al.*, in *Quantum Mesoscopic Phenomena and Mesoscopic Devices in Microelectronics*, I. O. Kulik, R. Ellialtıoglu, Eds. (Kluwer Academic Publishers, Dordrecht, 2000), pp. 429-438; cond-mat/9910062.
28. U. Eckern, G. Schön, and V. Ambegaokar *Phys. Rev. B* **30**, 6419 (1984).
29. T. H. Oosterkamp *et al.*, *Nature* **395**, 873 (1998).
30. A. J. Leggett *et al.*, *Rev. Mod. Phys.* **59**, 1 (1987); *Rev. Mod. Phys.* **67**, 725(E) (1995).
31. U. Weiss, *Quantum Dissipative Systems*, (World Scientific, Singapore, ed. 2, 1999).
32. M. Grifoni, E. Paladino, U. Weiss, *Eur. Phys. J. B* **10**, 719 (1999).
33. A. Abragam, *Principles of Nuclear Magnetism* (Oxford University Press, Oxford, 1961).
34. L. Tian, S. Lloyd, and T. P. Orlando, *Phys. Rev. B* **65**, 144516 (2002).
35. A. Garg, J. N. Onuchic, and V. Ambegaokar, *J. Chem. Phys.* **83**, 3391 (1985).
36. M. Tinkham, *Introduction to Superconductivity* (McGraw-Hill, Inc., New York, ed. 2, 1996).

37. P. Joyez, D. Vion, M. Götz, M. H. Devoret, D. Esteve, J. Supercond. **12**, 757 (1999).
38. A. Cottet, D. Vion, A. Aassime, P. Joyez, D. Esteve, and M.H. Devoret, Physica C **367**, 197 (2002).
39. A. Shnirman and G. Schön, Phys. Rev. B **57**, 15400 (1998).
40. M. H. Devoret and R. J. Schoelkopf, Nature **406**, 103 (2000).
41. A.B. Zorin, Physica C **368**, 284 (2002).
42. A.N. Korotkov and D.V. Averin, Phys. Rev. B **64**, 16531 (2001).
43. D. Vion, M. Götz, P. Joyez, D. Esteve, M. H. Devoret, Phys. Rev. Lett. **77**, 3435 (1996).
44. T.P. Orlando *et al.*, private communication, to be published.
45. H. Tanaka, Y. Sekine, S. Saito, and H. Takayanagi, Physica C **368**, 300 (2002).
46. W. Wernsdorfer, D. Mailly, A. Benoit, J. Appl. Phys. **87**, 5094 (2000).
47. M. Müick, J. B. Kycia, J. Clarke, Appl. Phys. Lett **78**, 96 (2001).
48. A. K. Jain, K. K. Likharev, J. E. Lukens, J. E. Sauvageat, Phys. Rep. **109**, 309 (1998).
49. D. S. Crankshaw, E. Trías, T. P. Orlando, IEEE Trans. on Appl. Superconductivity **11**, 1223 (2001).
50. M. H. Devoret, in *Quantum Fluctuations*, S. Reynaud, F. Giacobino, J. Zinn-Justin, Eds. (Elsevier Science, Amsterdam, 1997), pp. 351-386.
51. A similar decoupling to the measuring DC-SQUID based on symmetry can be realized with an additional flux-controlled coupling loop, see J. Clarke *et al.*, submitted to Physica Scripta.
52. U. Geigenmüller, J. Appl. Phys. **80**, 3934 (1996).
53. W. T. Coffey, Y. P. Kalmykov, J. T. Waldron, *The Langevin Equation; with Applications in Chemistry and Electrical Engineering*, (World Scientific, Singapore, 1996).
54. M. Feldman, private communications.
55. S. Kleff, S. Kehrein, and J. von Delft, to appear in Physica E.

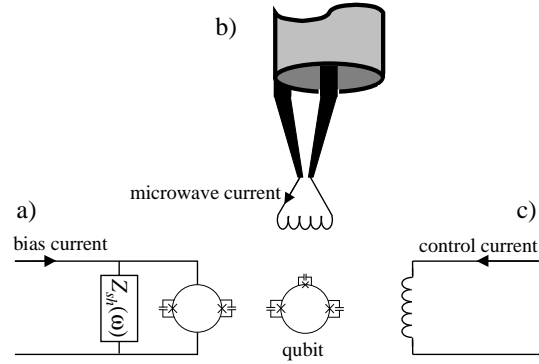


Fig. 1. Experimental setup for measurements on a Josephson persistent-current qubit. The qubit (center) is a superconducting loop that contains three Josephson junctions. It is inductively coupled to a DC-SQUID (a), and superconducting control lines for applying magnetic fields at microwave frequencies (b) and static magnetic fields (c). The DC-SQUID is realized with an on-chip shunt circuit with impedance Z_{sh} . The circuits a)-c) are connected to filtering and electronics (not drawn).

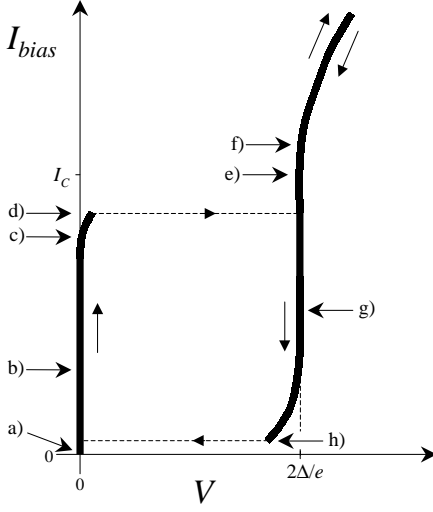


Fig. 2. Sketch of a typical hysteretic current-voltage characteristic (IV) for a current-biased Josephson junction or small DC-SQUID. The IV is hysteretic; arrows indicate which of the two branches is followed at an increase or decrease of the bias current. When the bias current I_{bias} is ramped up from zero (a), the voltage V first remains zero. The circuit is here on the supercurrent branch of the IV (b). When I_{bias} approaches the critical current I_C , a slow diffusive motion of the phase φ_{ext} leads to a very small voltage across the system (c). At slightly higher current (d), but always below I_C (e), the system switches to a running mode for φ_{ext} , and the voltage jumps to a value set by quasiparticle tunneling over the superconducting gap, $V = 2\Delta/e$ (this current level (d) is the switching current I_{SW}). At further increase of the current (f) the IV approaches an Ohmic branch, where transport is dominated by quasiparticle tunneling through the normal tunnel resistance of the junctions. When lowering the bias current the system follows the running mode (g) down to a low bias current where it retraps on the supercurrent branch (at the level I_{retrap} , indicated by (h)). See also the corresponding washboard potential model, in Fig. 3.

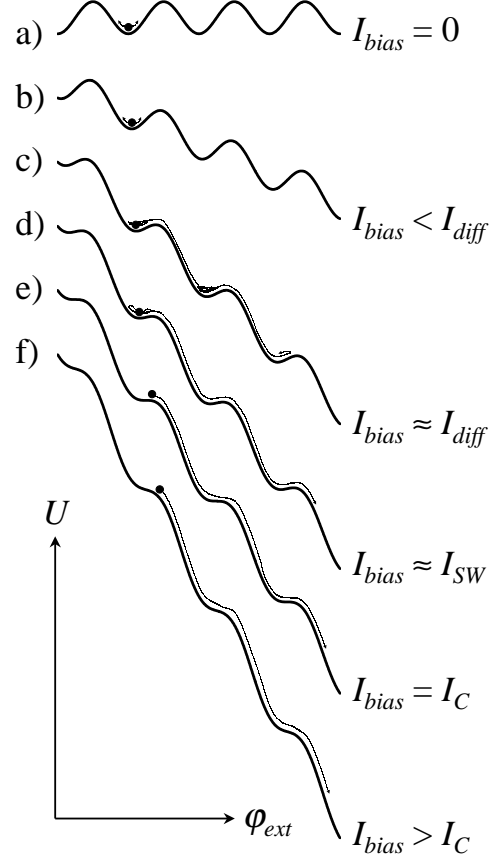


Fig. 3. The dynamics of a current-biased DC-SQUID, modeled as a particle with coordinate φ_{ext} in a one-dimensional tilted washboard potential U . The labeling a)-f) corresponds to that of Fig. 2. At zero (a) and small bias currents (b), the particle is trapped in a well of the washboard. Apart from the small plasma oscillations at the bottom of the well, the particle's coordinate φ_{ext} is fixed. When increasing the slope of the washboard, the particle will start to have a slow, on average downwards, diffusive dynamics, with rare excursions to one of the neighboring wells (c). At the switching current I_{SW} there is a high probability that the trapped particle will escape to a running mode (d), with effectively zero probability for retrapping. Here the loss of potential energy exceeds the dissipation when the particle moves one period down the washboard, and the particle builds up a high kinetic energy. Due to thermal fluctuations, external noise, and in certain cases quantum fluctuations, this occurs below the critical current I_C : the slope where all local minimums in the washboard potential disappear (e). At currents higher than this slope (f), the particle will always be in a running mode. The retrapping process when lowering the bias current follows similar dynamics.

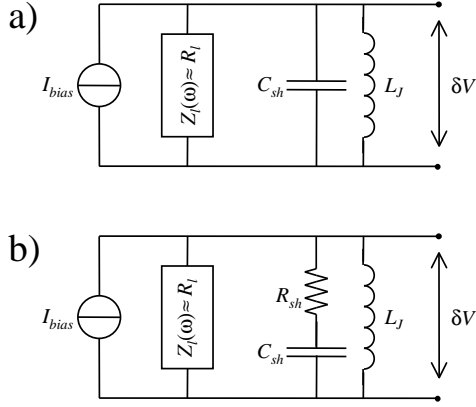


Fig. 4. Circuit models for the C -shunted DC-SQUID (a) and the RC -shunted DC-SQUID (b). The SQUID is modeled as an inductance L_J . A shunt circuit, the superconducting capacitor C_{sh} or the R_{sh} - C_{sh} series, is fabricated on chip very close to the SQUID. The noise that couples to the qubit results from Johnson-Nyquist voltage noise δV from the circuit's total impedance Z_t . Z_t is formed by a parallel combination of the impedances of the leads Z_l , the shunt and the SQUID, such that $Z_t = (1/Z_l + 1/(R_{sh} + 1/i\omega C_{sh}) + 1/i\omega L_J)^{-1}$, with $R_{sh} = 0$ for (a).

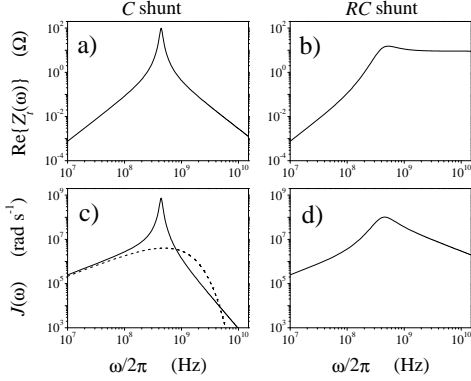


Fig. 5. A typical $\text{Re}\{Z_t(\omega)\}$ for the C -shunted SQUID (a) and the RC -shunted SQUID (b), and corresponding $J(\omega)$ in (c) and (d) respectively. For comparison, the dashed line in (c) shows a simple Ohmic spectrum (43) with exponential cut off $\omega_c/2\pi = 0.5$ GHz and $\alpha = 0.00062$. The parameters used here are $I_p = 500$ nA and $T = 30$ mK. The SQUID with $2I_{co} = 200$ nA is operated at $f = 0.75\pi$ and current biased at 120 nA, a typical value for switching of the C -shunted circuit (the RC -shunted circuit switches at higher current values). The mutual inductance $M = 8$ pH (i. e. $\frac{MI_p}{\Phi_0} = 0.002$). The shunt is $C_{sh} = 30$ pF and for the RC shunt $R_{sh} = 10 \Omega$. The leads are modeled by $R_l = 100 \Omega$.

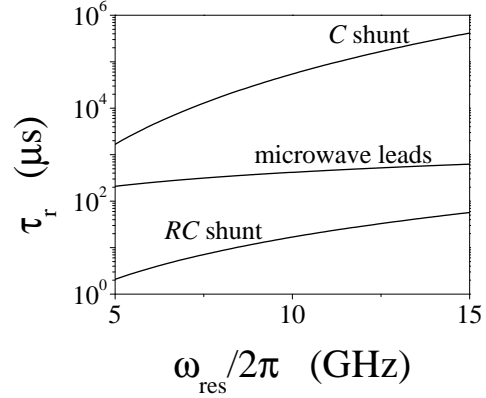


Fig. 6. Typical relaxation times due to the C -shunted SQUID, the RC -shunted SQUID, and coupling the microwave leads as a function of the resonance frequency at which the qubit is operated. The example of the microwave leads contribution is for a mutual inductance M_{mw} to the coaxial line of $M_{mw} = 0.1$ pH. Parameters are further as described in the caption of Fig. 5.

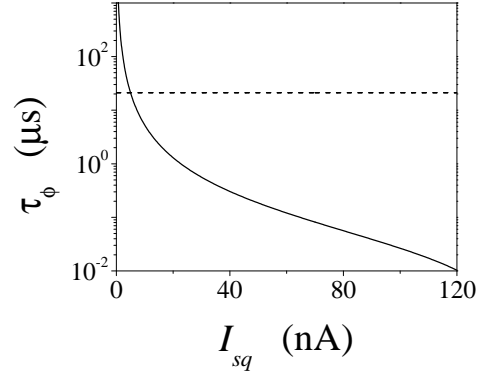


Fig. 7. The dephasing time (42) as a function of the bias current I_{sq} through the SQUID (solid line). The dashed line shows τ_ϕ for $I_{sq} = 5$ nA, a typical minimum value for the effective bias current for a SQUID with a few percent asymmetry between its junctions. At this point $\tau_\phi = 131 \mu\text{s}$, and $\alpha = 1 \cdot 10^{-7}$. Parameters are further as described in the caption of Fig. 5.

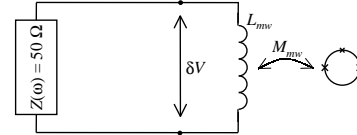


Fig. 8. Circuit model for coaxial line that is inductively coupled to the qubit. The coaxial line is modeled as a 50Ω impedance that is shorted near the qubit with an inductance L_{mw} . The qubit is coupled to this short with a mutual inductance M_{mw} . The noise that couples to the qubit results from Johnson-Nyquist voltage noise δV from the circuit's total impedance Z_t , formed by a parallel combination of the 50Ω impedance and L_{mw} .

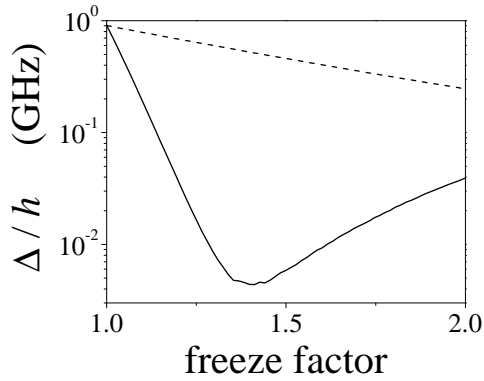


Fig. 9. Numerically simulated suppression of Δ in qubits where one (solid) or three (dashed) of the junctions are realized as small DC-SQUIDs, using typical qubit parameters as mentioned in the text. The horizontal axis is the factor by which the Josephson energy of the relevant junctions is increased. For the solid line, one can observe a non-monotonic dependence of Δ on the freeze factor, which results from the fact that if the Josephson coupling of the weak junction is strongly increased, alternative tunneling paths between the current states open up, see also Ref. [19].